JOURNAL OF THEORETICAL
AND APPLIED MECHANICS
64, 3, pp. 245–256, Warsaw 2026
https://doi.org/10.15632/jtam-pl/226037

ANALYSIS OF VIBRATION CHARACTERISTICS OF POROUS FUNCTIONALLY GRADED CONICAL SHELL IN THERMAL ENVIRONMENTS

Runhao WAN[1*], Wenguang LIU[2]

[1] *School of Advanced Manufacturing, Nanchang University, Nanchang, China*
[2] *School of Aeronautical Manufacturing and Mechanical Engineering, Nanchang Hangkong University, Nanchang, China*
*corresponding author, *wanrunhao@email.ncu.edu.cn*

This study investigates the free vibration modal frequencies of a metal-ceramic functionally graded porous conical shell under thermal loading. Temperature-dependent material properties and two porosity distribution patterns, namely uniform and non-uniform porosity distributions, are considered. Based on the Sanders shell theory and the Rayleigh–Ritz method with Chebyshev polynomials, the model is verified by FEM within 5.04 % error. Parametric analysis shows that temperature dominates at low wave numbers, while porosity governs at high wave numbers. Increasing the S-shaped volume fraction exponent raises frequencies and weakens thermal effects, providing a theoretical basis for high-temperature engineering applications.

Keywords: porosity; thermal loading; Chebyshev polynomials; functionally graded conical shell; modal frequencies.

1. Introduction

Functionally graded materials (FGMs) are advanced composites with continuous spatial variations in composition, microstructure and properties. Owing to their high heat resistance, high strength, and lightweight characteristics, FGMs can effectively alleviate thermal-stress concentrations (Asemi & Jedari Salami, 2015; Kołakowski & Teter, 2016; Kalali *et al.*, 2016; Pillai & Rahaman, 2026; Ding & Li, 2008; Chumanov *et al.*, 2015). Therefore, FGMs have broad application prospects in aerospace and mechanical engineering.

Conical shells are widely used in aircraft fuselages, vessel propulsion systems, and other load-bearing structures that often operate in complex multi-field coupled environments. Consequently, the design and analysis of FGM conical shells have attracted considerable research attention. As advanced composite structures, FGMs may contain internal defects such as pores owing to limitations in manufacturing technologies. The presence of pores not only affects the material's acoustic properties and thermal conductivity but also influences its mechanical behavior. In recent years, a mounting number of scholars have commenced exploring the influence of material porosity on the mechanical behavior of FGM shells. Grounded in the geometrically nonlinear Kirchhoff–Love thin shell constitutive model, Feng and Hu (2026) examined the dynamic behavior of porous ferromagnetic FGM cylindrical shells under armature action. Within the framework of the first-order shear deformation theory, Xue *et al.* (2023) explored the free vibration behavior of porous FGM cylindrical panels and shells. Adopting the sinusoidal shear deformation theory and the Rayleigh–Ritz method, Wang and Wu (2017) examined the free vibration characteristics of FGM shells under different porosity distribution patterns. Applying an innovative semi-analytical method, Li *et al.* (2019) explored the free vibration behavior of porous FGM shells under arbitrary boundary conditions.

FGMs have also received extensive attention in high-temperature engineering applications since their initial proposal by Japanese researchers in the 1980s. Reddy (2000) analyzed the bending and vibration of FGM plates under thermal loads using a higher-order shear deformation theory, considering the temperature-dependent nonlinear variation of material properties. Matsunaga (2009) assessed the thermal buckling of FGM shells via a higher-order theory, emphasizing the coupling effect between boundary conditions and the gradient index. Concerning dynamic feedback, Huang and Shen (2004) examined the impacts of thermal surroundings on the nonlinear vibration characteristics of FGM shells. They discovered that temperature rise generally leads to a decrease in natural frequency, though the gradient distribution can modulate this trend. Mallek *et al.* (2025) considered two distinct porosity distribution patterns and conducted a comprehensive analysis on the porosity effects of porous FGMs.

Limited studies have addressed the free vibration of porous FGM conical shells under thermal loading. Therefore, this study develops a semi-analytical model based on the Sanders shell theory and the Rayleigh–Ritz method. Temperature-dependent material properties and different porosity distributions are incorporated through the Voigt model to examine the effects of thermal gradients, porosity, and material gradation on modal frequencies.

2. Geometry model

As depicted in Fig. 1, it is assumed that the boundary conditions at the endpoints of the FGM conical shell are simulated by artificial springs. The geometric parameters of the conical shell include: length L, thickness h, the radius of the small end is R_1 and the radius of the large end is R_2, the semi-cone angle is a_0. The material properties of the FGM conical shell vary continuously and gradually only through the thickness, an inherent material characteristic unchanged during vibration analysis. The outer surface of the conical shell is pure metal, and the inner surface is pure ceramic. An orthogonal surface coordinate system (x, θ, z) is established at the mid-surface of the conical shell, as shown in Fig. 1. The x, θ, z represent the axial, circumferential and thickness direction, respectively. The displacement components in the x, θ, and z directions of the coordinate system are represented by u, v, and w, respectively.

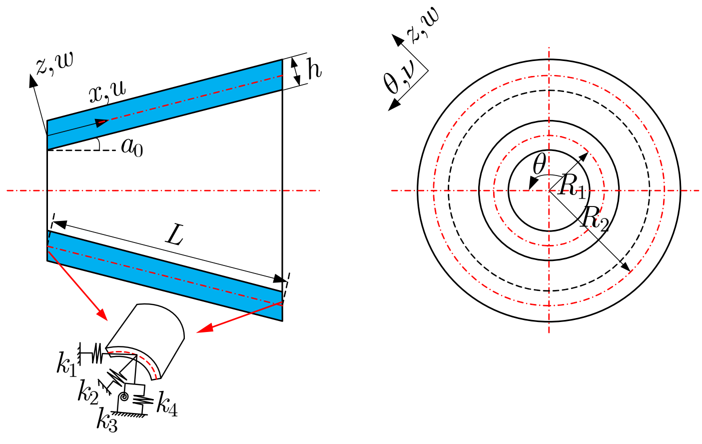

Fig. 1. Geometric model and coordinate system of a porous FGM conical shell: x – axial direction, θ – circumferential direction, z – thickness direction, R_1 – small-end radius, R_2 – large-end radius, L – length, a_0 – semi-cone angle.

The radius at any point on the shell's mid-surface varies along the axial coordinate x (Wan *et al.*, 2025b):

$$R(x) = R_1 + x \sin(\alpha_0), \qquad 0 \le x \le L. \tag{2.1}$$

3. Thermophysical properties of FGMs

Two typical porosity distributions along the thickness are considered: even porosity (model I) and uneven porosity (model II), as illustrated in Fig. 2. Within the framework of the Voigt model, the effective material property of FGMs with different pore distribution patterns is given as follows (Wang *et al.*, 2018):

$$
\begin{aligned}
&P_{\mathrm{eff}}^{\mathrm{I}}(x,z) = (P_m - P_c)V_m + \frac{\gamma}{2}(P_c + P_m),\\
&P_{\mathrm{eff}}^{\mathrm{II}}(x,z) = (P_m - P_c)V_m + P_c - \frac{\lambda}{2}\left(1 - 2\frac{|z|}{h}\right)(P_c + P_m),
\end{aligned}
\tag{3.1}
$$

where $P_{\mathrm{eff}}^{\mathrm{I}}$ and $P_{\mathrm{eff}}^{\mathrm{II}}$ denote the effective material property P of the FGMs for porosity models I and II, respectively. In this study, P represents the effective elastic modulus E_{eff}, Poisson's ratio ν_{eff}, density ρ_{eff}, thermal expansion coefficient α_{eff}, or thermal conductivity coefficient k_{eff}. The parameter γ denotes the porosity volume fraction, V_m denotes the metal volume fraction, and the subscripts c and m refer to ceramic and metal, respectively.

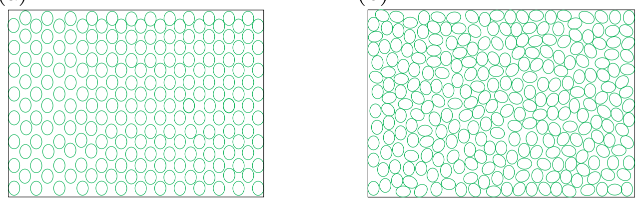

Fig. 2. Pore distribution: (a) even porosity, (b) uneven porosity.

To realize a gradual and continuous evolution of internal stresses within FGMs, Chi and Chung (2006) proposed a Sigmoid-type piecewise volume fraction:

$$
\begin{aligned}
&V_{1m}(z) = 1 - \frac{1}{2}\left(\frac{h/2 - z}{h/2}\right)^N, \qquad 0 \le z \le h/2,\\
&V_{2m}(z) = \frac{1}{2}\left(\frac{h/2 + z}{h/2}\right)^N, \qquad 0 \le z \le h/2,
\end{aligned}
\tag{3.2}
$$

where N is the volume-fraction exponent controlling the material gradation through the thickness. The functions $V_{1m}(z)$ and $V_{2m}(z)$ denote the metal volume fractions in the upper half-thickness interval ($0 \le z \le h/2$) and lower half-thickness interval ($-h/2 \le z \le 0$), respectively.

Considering the temperature dependence of the physical properties of FGMs, the material parameters can be expressed as (Shen, 2012):

$$
P_{c,m} = p_0\left(p_{-1}T^{-1} + 1 + p_1T + p_2T^2 + p_3T^3\right),
\tag{3.3}
$$

where $P_{c,m}$ represents the thermal property parameters of the material; p_0, p_{-1}, p_1, p_2, p_3 are the temperature-sensitive characteristic coefficients of the material, with specific values as shown in Table 1.

Under thermal conditions, a nonlinear temperature distribution is assumed through the thickness of an FGM conical shell. The inner surface ($z = -h/2$) is at temperature T_c, and the outer surface ($z = h/2$) is at $T_m = 300\,\mathrm{K}$ (ambient). In the stress-free state, the thickness-dependent temperature rise $T(z)$ is derived from the steady-state heat conduction equation and thermal boundary conditions:

$$
\begin{aligned}
&T(z) = T_c - T_{cm}\xi(z,h),\\
&-\frac{\mathrm{d}}{\mathrm{d}z}\left[k_{\mathrm{eff}}(z)\frac{\mathrm{d}T}{\mathrm{d}z}\right] = 0,
\end{aligned}
\tag{3.4}
$$

Table 1. Temperature-dependent coefficients of ZrO_2-SUS304 (Liu *et al.*, 2017).

Properties	Material	p_{-1}	p_0	p_1	p_2	p_3
ρ [$\mathrm{kg \cdot m^{-3}}$]	SUS304	0	8166	0	0	0
	ZrO_2	0	3657	0	0	0
E [GPa]	SUS304	0	201.04	3.079×10^{-4}	-6.534×10^{-4}	0
	ZrO_2	0	132.20	-3.805×10^{-4}	-6.127×10^{-4}	0
v	SUS304	0	0.3262	-2.002×10^{-4}	3.797×10^{-4}	0
	ZrO_2	0	0.3330	0	0	0
a [$\mathrm{K^{-1}}$]	SUS304	0	12.3×10^{-6}	8.086×10^{-6}	0	0
	ZrO_2	0	13.3×10^{-6}	-1.421×10^{-3}	9.549×10^{-7}	0
k [$\mathrm{W/m \cdot K}$]	SUS304	0	12.04	0	0	0
	ZrO_2	0	1.78	0	0	0

where $T_{cm} = T_c - T_m$ represents the temperature difference across the inner and outer surfaces of the shell. The solution form of the function $\xi(z,h)$ was obtained by Wu (2004) as a polynomial series:

$$\xi(z,h) = \frac{\dfrac{2z+h}{2h} + \displaystyle\sum_{i=1}^{5} \frac{-1}{iN+1} \left(\frac{k_{cm}}{k_m}\right)^i \left(\frac{2z+h}{2h}\right)^{iN+1}}{1 + \displaystyle\sum_{i=1}^{5} \left[\frac{(-1)^i}{iN+1} \left(\frac{k_{cm}}{k_m}\right)^i\right]}, \tag{3.5}$$

where $k_{cm} = k_c - k_m$, and k_c and k_m denote the thermal conductivity coefficients of the ceramic and metal, respectively.

4. Energy equation of an FGM conical shell

The Sanders shell theory is employed to derive the strain-displacement relations for an FGM conical shell, with the following basic assumptions: (1) the straight normal to the shell mid-surface remains straight after deformation but is not necessarily normal to it; (2) the transverse normal stress is negligible; (3) in-plane strains and normal rotations are small; (4) the shell thickness is much smaller than its characteristic dimensions.

Based on the Sanders shell theory, the relations between the in-plane strains and displacement components of a conical shell can be derived as follows (Loy & Lam, 1997):

$$\begin{gathered}
\varepsilon_x = \varepsilon_1 - z\varepsilon_4, \qquad \varepsilon_\theta = \varepsilon_2 - z\varepsilon_5, \qquad \varepsilon_{x\theta} = \varepsilon_3 - 2z\varepsilon_6, \\
\{\varepsilon_1, \varepsilon_2, \varepsilon_3\} = \left\{\frac{\partial u}{\partial x}, \ \frac{1}{R}\left(\frac{\partial v}{\partial \theta} + w\right), \ \frac{\partial v}{\partial x} + \frac{1}{R}\frac{\partial u}{\partial \theta}\right\}, \\
\{\varepsilon_4, \varepsilon_5\} = \left\{\frac{\partial^2 w}{\partial x^2}, \ \frac{1}{R^2}\left(\frac{\partial^2 w}{\partial \theta^2} - \frac{\partial v}{\partial \theta}\right)\right\}, \\
\{2\varepsilon_6\} = \left\{\frac{1}{R}\left(\frac{2\partial^2 w}{\partial x \partial \theta} + \frac{1}{2R}\frac{\partial u}{\partial \theta} - \frac{3}{2}\frac{\partial v}{\partial x}\right)\right\},
\end{gathered} \tag{4.1}$$

where ε_x and ε_θ represent the normal strains in the x and θ directions, respectively; $\varepsilon_{x\theta}$ denotes the shear strain within the $x\theta$ plane; ε_1, ε_2, and ε_3 are the surface strain components of the mid-surface; ε_4, ε_5, and ε_6 represent the curvatures of the mid-surface.

The stress-strain constitutive relation is formulated as

$$\begin{Bmatrix} \sigma_x \\ \sigma_\theta \\ \sigma_{x\theta} \end{Bmatrix} = \begin{pmatrix} Q_{11} & Q_{12} & 0 \\ Q_{12} & Q_{22} & 0 \\ 0 & 0 & Q_{33} \end{pmatrix} \begin{Bmatrix} \varepsilon_x \\ \varepsilon_\theta \\ \varepsilon_{x\theta} \end{Bmatrix}, \tag{4.2}$$

where σ_x and σ_θ denote the normal stresses in the x and θ directions, respectively; $\sigma_{x\theta}$ is the shear stress in the $x\theta$ plane; Q_{jk} $(j,k = 1,2,3)$ represents the reduced stiffness constants, defined as

$$\begin{aligned} &Q_{11}(s) = Q_{22}(s) = \frac{E^1_{\mathrm{eff}}(s)}{1 - v^1_{\mathrm{eff}}(s)}, \qquad Q_{12}(s) = \frac{v^1_{\mathrm{eff}}(s) E^1_{\mathrm{eff}}(s)}{1 - v^1_{\mathrm{eff}}(s)}, \\ &\qquad\qquad Q_{33}(s) = \frac{E^1_{\mathrm{eff}}(s)}{2(1 + v^1_{\mathrm{eff}}(s))}, \qquad 0 \le z \le h/2, \\ &Q_{11}(s) = Q_{22}(s) = \frac{E^2_{\mathrm{eff}}(s)}{1 - v^2_{\mathrm{eff}}(s)}, \qquad Q_{12}(s) = \frac{v^2_{\mathrm{eff}}(s) E^2_{\mathrm{eff}}(s)}{1 - \left(v^2_{\mathrm{eff}}(s)\right)^2}, \\ &\qquad\qquad Q_{33}(s) = \frac{E^2_{\mathrm{eff}}(s)}{2\left[1 - \left(v^2_{\mathrm{eff}}(s)\right)^2\right]}, \qquad -h/2 \le z \le 0, \end{aligned} \tag{4.3}$$

where $s = 1$ for $0 \le z \le h/2$ and $s = 2$ for $-h/2 \le z \le 0$.

The resultant force and resultant moment acting on the FGM shell are

$$\{N\,, M\} = \begin{Bmatrix} N_x \\ N_\theta \\ N_{x\theta} \\ M_x \\ M_\theta \\ M_{x\theta} \end{Bmatrix} = \{\varepsilon\}\,[\mathbf{V}] = \begin{Bmatrix} \varepsilon_1 \\ \varepsilon_2 \\ \varepsilon_3 \\ \varepsilon_4 \\ \varepsilon_5 \\ 2\varepsilon_6 \end{Bmatrix} \begin{bmatrix} A_{11} & A_{12} & 0 & -B_{11} & -B_{12} & 0 \\ A_{12} & A_{22} & 0 & -B_{12} & -B_{22} & 0 \\ 0 & 0 & A_{33} & 0 & 0 & -B_{33} \\ B_{11} & B_{12} & 0 & -D_{11} & -D_{12} & 0 \\ B_{12} & B_{22} & 0 & -D_{12} & -D_{22} & 0 \\ 0 & 0 & B_{33} & 0 & 0 & -D_{33} \end{bmatrix}, \tag{4.4}$$

where N_x, N_θ, $N_{x\theta}$ are the in-plane resultant forces in the x, θ, and $x\theta$ directions, M_x, M_θ, $M_{x\theta}$ are the resultant bending and torsion moments in the corresponding directions; $\{\varepsilon\}$ denotes the strain vector. The coefficients A_{jk}, B_{jk}, D_{jk} $(j,k = 1,2,3)$ are global, through-thickness integrated stiffness coefficients representing extensional stiffness, extension-bending coupling stiffness, and bending stiffness, respectively. These coefficients incorporate the effects of material gradation, porosity distribution, and temperature-dependent material properties, with no simplifications adopted in the derivation.

Based on the Sanders theory, the strain energy U and kinetic energy K of the FGM shell are obtained as follows:

$$\begin{aligned} U &= \frac{1}{2} \int_0^L \int_0^{2\pi} \{\boldsymbol{\varepsilon}\}^{\mathrm{T}} [\mathbf{V}] \{\boldsymbol{\varepsilon}\} R \,\mathrm{d}x \,\mathrm{d}\theta, \\ K &= \frac{1}{2} \int_0^l \int_0^{2\pi} \rho_{\mathrm{T}} \left[\left(\frac{\partial u}{\partial t}\right)^2 + \left(\frac{\partial v}{\partial t}\right)^2 + \left(\frac{\partial w}{\partial t}\right)^2 \right] R \,\mathrm{d}x \,\mathrm{d}\theta, \end{aligned} \tag{4.5}$$

where ρ_{T} denotes the mass density per unit length, which is expressed as

$$\rho_{\mathrm{T}} = \int_0^{h/2} \rho^1_{\mathrm{eff}}(z) \,\mathrm{d}z + \int_{-h/2}^{0} \rho^2_{\mathrm{eff}}(z) \,\mathrm{d}z. \tag{4.6}$$

The elastic strain energy stored in the boundary spring of an FGM shell is given by

$$
\begin{aligned}
V = {} & \frac{1}{2}\int_0^{2\pi}\left[k_1u^2 + k_2v^2 + k_3w^2 + k_4\left(\frac{\partial w}{\partial x}\right)^2\right]_{x=0} R_1(0)\,\mathrm{d}\theta \\
& + \frac{1}{2}\int_0^{2\pi}\left[k_1u^2 + k_2v^2 + k_3w^2 + k_4\left(\frac{\partial w}{\partial x}\right)^2\right]_{x=L} R_2(L)\,\mathrm{d}\theta,
\end{aligned} \tag{4.7}
$$

where k_1, k_2, k_3, and k_4 represent the axial spring stiffness, circumferential spring stiffness, radial spring stiffness, and rotational spring stiffness, respectively.

5. Characteristic equation of an FGM conical shell

The axial, circumferential, and radial displacements of the FGM conical shell are periodic functions of the circumferential angle θ with a period of 2π, requiring simultaneous solution. Consequently, the displacement fields are expressed in the form of trigonometric functions associated with the circumferential modal number and the circumferential wave number

$$
\begin{aligned}
u(x,\theta,t) &= U_n(x)\cos(n\theta + \omega t), \\
v(x,\theta,t) &= V_n(x)\sin(n\theta + \omega t), \\
w(x,\theta,t) &= W_n(x)\cos(n\theta + \omega t),
\end{aligned} \tag{5.1}
$$

where $U_n(x)$, $V_n(x)$, and $W_n(x)$ denote the mode functions at azimuthal wave number n, and ω represents the modal frequencies. As documented in (Xu *et al.*, 2024), Chebyshev polynomials exhibit favorable convergence properties, thus permitting their expansion into different-order modes

$$
\begin{aligned}
U_n(x) &= \sum_{m=0}^{M} A_m T_m(x), \\
V_n(x) &= \sum_{m=0}^{M} B_m T_m(x), \\
W_n(x) &= \sum_{m=0}^{M} C_m T_m(x),
\end{aligned} \tag{5.2}
$$

where m denotes the axial wave number and n denotes the circumferential wave number; A, B, and C are undetermined coefficients, and M is the truncation order. $T(\cdot)$ stands for the Chebyshev polynomial, whose specific expression is

$$
\begin{aligned}
& T_0(x) = 1, \qquad T_1(x) = x, \\
& T_{a+1}(x) = 2x\cdot T_a(x) - T_{a-1}(x), \qquad a \geq 1, \qquad a \in \mathrm{N}^+.
\end{aligned} \tag{5.3}
$$

On the basis of the above energy expression, the energy model can be established as

$$
\mathit{\Pi} = U_{\max} + V_{\max} - K_{\max}, \tag{5.4}
$$

where subscript "max" denotes the maximum value of each energy term during one period of harmonic vibration, which is a standard treatment in the Rayleigh–Ritz method for free vibration analysis.

By virtue of the Rayleigh–Ritz method, partial differentiation with respect to the undetermined coefficients is performed to establish the vibration control equations

$$\left[\omega^2\mathbf{M}_1 + 2\mathbf{M}_2 - \mathbf{K}\right]\begin{Bmatrix} U \\ V \\ W \end{Bmatrix} = 0, \tag{5.5}$$

where $\mathbf{K}$, $\mathbf{M}_1$ and $\mathbf{M}_2$, denote the stiffness, inertial mass matrix and coupled mass matrix, respectively. U, V, and W denote the undetermined coefficient vectors, with the specific expressions given by

$$\begin{aligned} U &= \{U_0, U_1, U_2, ..., U_M\}^{\mathrm{T}}, \\ V &= \{V_0, V_1, V_2, ..., V_M\}^{\mathrm{T}}, \\ W &= \{W_0, W_1, W_2, ..., W_M\}^{\mathrm{T}}. \end{aligned} \tag{5.6}$$

6. Boundary conditions for an FGM conical shell

The boundary conditions at both ends of the conical shell are modeled by artificial springs with stiffness coefficients k_1 (axial), k_2 (circumferential), k_3 (radial), and k_4 (rotational). Conventional boundary conditions comprise free (F), clamped (C), and simply supported (S) ones. The spring stiffness values are assigned in accordance with the settings given in Table 2 (Chen *et al.*, 2023).

Table 2. Artificial spring stiffness value.

Boundary conditions	Free	Clamped	Simply supported
Spring stiffness value	$k_1 = 0$	$k_1 = 10^{14}$	$k_1 = 0$
	$k_2 = 0$	$k_2 = 10^{14}$	$k_2 = 10^{14}$
	$k_3 = 0$	$k_3 = 10^{14}$	$k_3 = 10^{14}$
	$k_4 = 0$	$k_4 = 10^{14}$	$k_4 = 0$

7. Results and discussion

To facilitate subsequent analysis, the frequency is rendered dimensionless as given in Eq. (7.1) (Wan *et al.*, 2025a):

$$\omega_1 = \omega R_2\sqrt{\rho_m(1-\nu_m^2)/E_m}, \tag{7.1}$$

where E_m, ν_m, and ρ_m are all material properties of the metal.

Unless otherwise stated, the geometric parameters of the conical shell adopted in the numerical analysis are defined as follows: $h = 0.001\,\mathrm{m}$, $R_1 = 0.2\,\mathrm{m}$, $R_2 = 1.195\,\mathrm{m}$, $L = 2\,\mathrm{m}$, $a_0 = 30°$. The volume fraction exponent $N = 1$, temperature difference $T_{cm} = 700\,\mathrm{K}$, and the axial wave number m and circumferential wave number n are both 1.

Table 3 presents the variation in modal frequencies with circumferential and axial wave numbers for a pore-free FGM shell under clamped-free boundary conditions. The results demonstrate that the modal frequencies computed from Eq. (5.5) are in close agreement with those obtained from finite element analysis (FEM), with all discrepancies lying within an acceptable range. This confirms the validity of the modal frequency equation for an FGM shell. FEM model validation is conducted using ABAQUS 2022. A converged mesh of 0.02 m is used, containing 12 000 elements and 15 600 nodes. Temperature-dependent ZrO_2-SUS304 properties are applied, and two

Table 3. Dimensionless modal frequencies of a conical shell with a C-F boundary.

(n,m)	(1,2)	(1,3)	(1,4)	(1,5)
Present	0.088	0.113	0.254	0.331
FEM	0.091	0.119	0.257	0.335
Error [%]	3.29	5.04	1.16	1.19
Modal shape	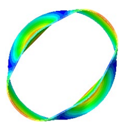	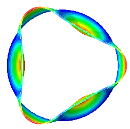	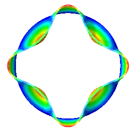	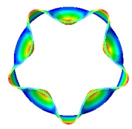
(n,m)	(1,6)	(1,7)	(1,8)	(1,9)
Present	0.453	0.512	0.622	0.735
FEM	0.460	0.524	0.635	0.741
Error [%]	1.52	2.29	2.04	0.81
Modal shape	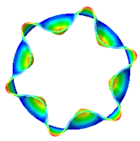	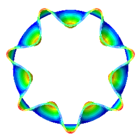	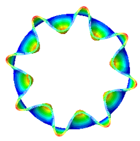	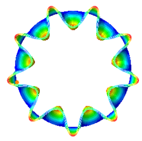

porosity distributions are simulated via the Voigt model. Clamped-clamped boundary conditions are imposed on both ends of the conical shell, matching the theoretical model.

Figure 3 shows the effect of temperature difference on the modal frequencies of an FGM shell at different porosity volume fractions. For low-order modes with $(m,n) < 3$, global bending and stretching dominate. Temperature reduces the FGM effective elastic modulus, decreasing structural stiffness and modal frequencies. For higher-order modes at $(m,n) = 3$, local deformation prevails. Geometric constraints offset temperature effects, making its influence on modal frequencies negligible. However, the influence of γ on modal frequencies increases as the vibration wave numbers (m,n) grow. When T_{cm} is constant, the modal frequencies of FGMs increase with increasing γ; when γ equals zero, the modal frequency of the pore model I conical shell equals that of the pore model II conical shell; when γ is non-zero, the modal frequency of pore model I is always greater than that of pore model II, whilst the rate of increase for pore model I modal frequencies is also higher than that for pore model II modal frequencies, mainly due to its lower effective mass density. As vibration theory indicates, frequency is inversely proportional to the square root of mass. Although model II has a slightly higher elastic modulus, the effect of mass reduction dominates, leading to higher frequencies for model I. The contribution of pore model I voids to the modal frequencies increase due to mass reduction is greater than the contribution of pore model II voids to the modal frequencies increase due to stiffness enhancement. The mass reduction does not directly increase stiffness. Model I shows a remarkable decrease in mass with a slight drop in stiffness. Model II presents a slight increase in stiffness with a minor decrease in mass.

Figure 4 illustrates the effect of temperature difference on the modal frequencies of a porous FGM shell for different volume fraction indices. The two porosity models show similar trends, although the numerical values differ. When T_{cm} is small, the influence of N on the modal frequencies is weak. As T_{cm} increases, the effect of N on modal frequencies becomes more pronounced, especially for smaller values of N. The relationship between N and modal frequencies is not strictly monotonic over the entire range examined. Among the values considered in this study, the modal frequency decreases from $N = 0$ to $N = 0.5$ and then increases as N increases from 0.5 to 10; therefore, $N = 0.5$ gives the minimum modal frequency in the present parametric study. At $N = 0$, each plane perpendicular to the thickness direction contains 50 %

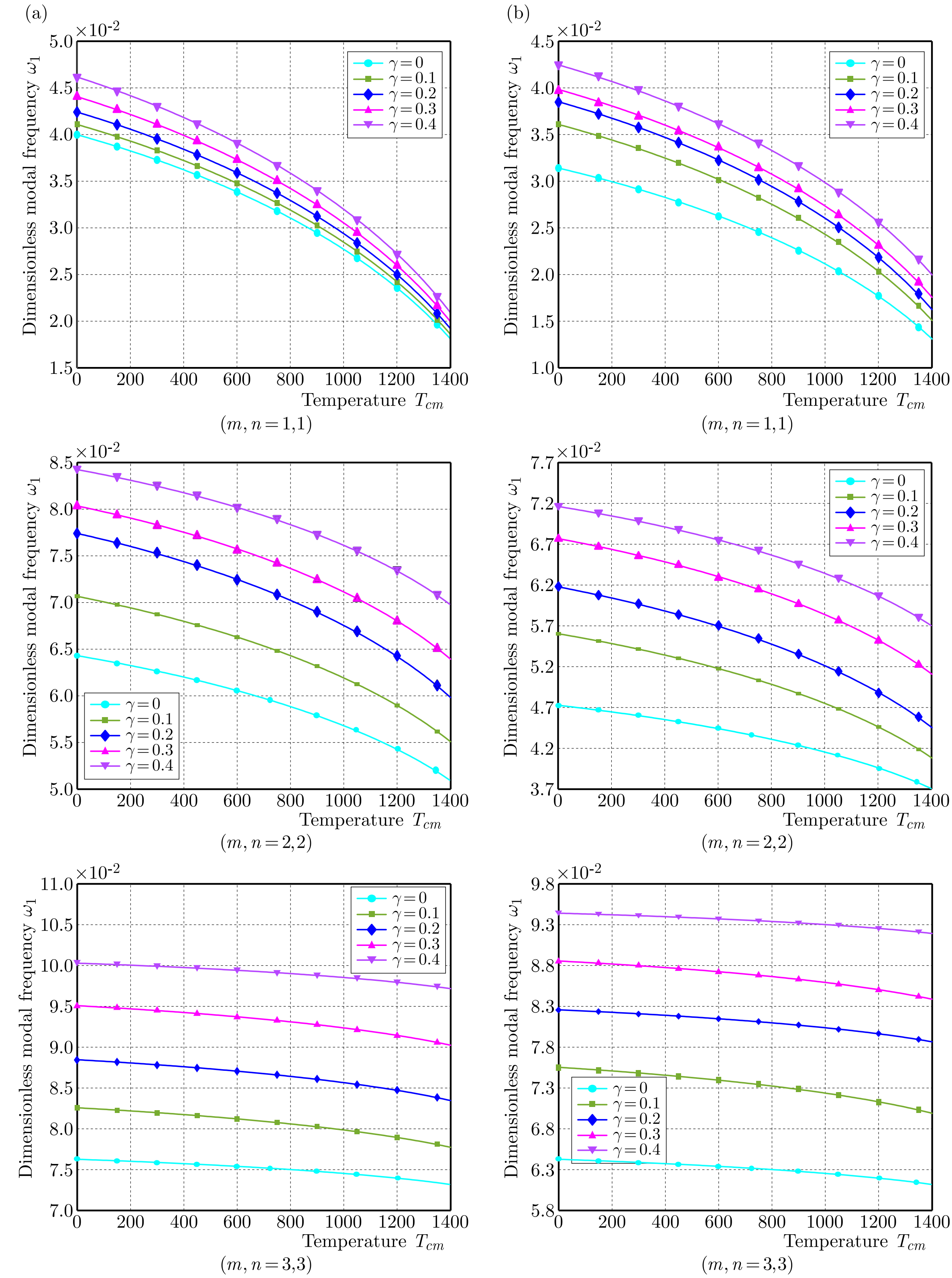

Fig. 3. Effect of temperature difference on dimensionless modal frequencies of an FGM shell at different pore volume fractions (the dimensionless definition of ω_1 is given in Eq. (7.1)): (a) even porosity; (b) uneven porosity.

metal and 50 % ceramic. As N increases beyond 0.5, the ceramic content near the inner high-temperature surface increases while the metallic content near the outer surface also increases. Because the ceramic phase has better thermal resistance than the metallic phase, increasing N

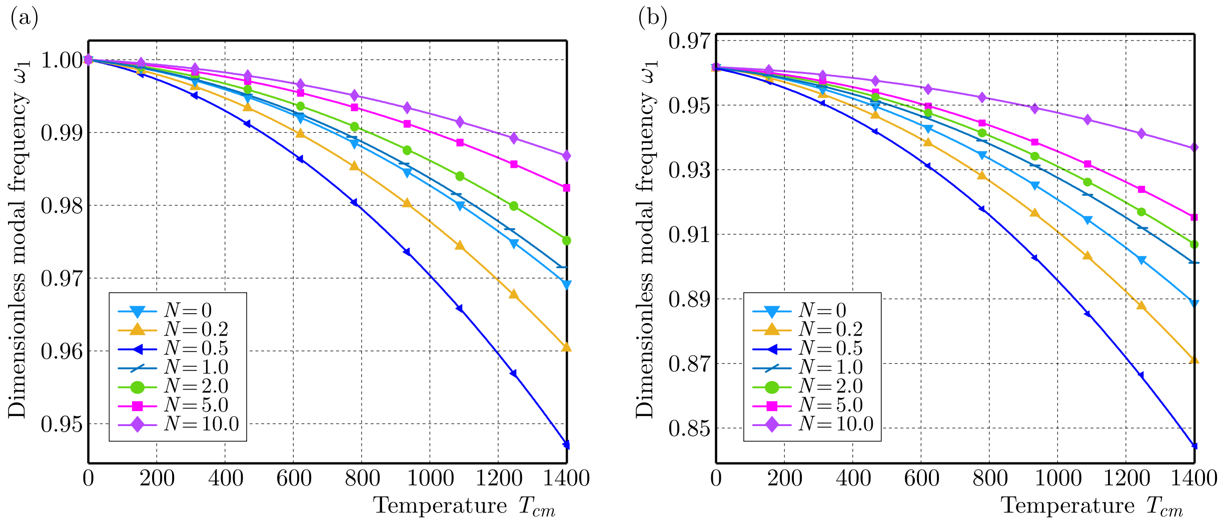

Fig. 4. Effect of temperature difference on dimensionless modal frequencies of an FGM shell at different volume fraction indexes: (a) even porosity; (b) uneven porosity.

beyond the minimum-frequencies point reduces the sensitivity of the conical shell stiffness to the temperature difference. Accordingly, an S-shaped piecewise volume-fraction distribution with an appropriately selected exponent can help reduce thermal sensitivity while retaining sufficient metallic content for structural strength.

8. Conclusion

In this paper, the free vibration equations of a porous metal-ceramic functionally graded conical shell were derived based on the Sanders thin-shell theory and the Rayleigh–Ritz method. The variation trends of modal frequencies under thermal loading were then examined. The main conclusions are summarized as follows:

1) At the same porosity volume fraction, pore model I yields a larger increase in modal frequencies than pore model II within the considered parameter range, mainly because model I produces a more significant reduction in effective mass density. Therefore, when the primary design objective is to increase modal frequencies through mass reduction, pore model I may be advantageous for the cases investigated in this study. However, in engineering practice, the selection between the two porosity distributions should also consider strength, stability, manufacturing feasibility, and other service requirements.
2) At low vibration wave numbers, the temperature difference has a more pronounced influence on the modal frequencies of an FGM shell than the porosity volume fraction, whereas at high vibration wave numbers, porosity becomes the dominant factor. For the S-shaped piecewise volume-fraction distribution considered in this study, the modal frequencies reach their minimum at $N = 0.5$ among the examined volume-fraction exponents and then increase as N increases from 0.5 to 10. Increasing the exponent beyond this minimum-frequencies point can mitigate the influence of the temperature difference on shell stiffness while maintaining metallic components that contribute to structural strength. This feature is beneficial for long-term service in variable high-temperature thermal environments with an arbitrary inner-surface temperature.
3) The present theoretical model does not include thermal stress and its coupling effect on modal frequencies. Future work will establish a thermo-mechanical coupling dynamic model to evaluate the effect of thermal stress and thereby improve prediction accuracy and applicability.

Acknowledgments

The authors are very grateful to the anonymous reviewers for their constructive comments, and gratefully acknowledge the financial support from the National Natural Science Foundation of China (grant no. 52365012) and the Natural Science Foundation of Jiangxi Province (grant no. 20224ACB204015).

References

1. Asemi, K., & Jedari Salami, S. (2015). A study on low velocity impact response of FGM rectangular plates with 3D elasticity based graded finite element modeling. *Journal of Theoretical and Applied Mechanics*, *53*(4), 859–872. https://doi.org/10.15632/jtam-pl.53.4.859
2. Chen, Y.G., Wang, Q.S., Zhong, R., Shi, X.J., & Qin, B. (2023). Fiber orientation and boundary stiffness optimization of laminated cylindrical shells with elastic boundary for maximum the fundamental frequency by an improved sparrow search algorithm. *Thin-Walled Structures*, *193*, Article 111299. https://doi.org/10.1016/j.tws.2023.111299
3. Chi, S.-H., & Chung, Y.-L. (2006). Mechanical behavior of functionally graded material plates under transverse load–Part I: Analysis. *International Journal of Solids and Structures*, *43*(13), 3657–3674. https://doi.org/10.1016/j.ijsolstr.2005.04.011
4. Chumanov, I.V., Anikeev, A.N., & Chumanov, V.I. (2015). Fabrication of functionally graded materials by introducing wolframium carbide dispersed particles during centrifugal casting and examination of FGM's structure. *Procedia Engineering*, *129*, 816–820. https://doi.org/10.1016/j.proeng.2015.12.111
5. Ding, S.H., & Li, X. (2008). An anti-plane shear crack in bonded functionally graded piezoelectric materials under electromechanical loading. *Computational Materials Science*, *43*(2), 337–344. https://doi.org/10.1016/j.commatsci.2007.11.009
6. Feng, J.B., & Hu, Y.D. (2026). Three-dimensional magneto-thermoelastic coupling resonance of spinning functionally graded cylindrical shells with porosity. *Thin-Walled Structures*, *219*(Part A), Article 114175. https://doi.org/10.1016/j.tws.2025.114175
7. Huang, X.-L., & Shen, H.-S. (2004). Nonlinear vibration and dynamic response of functionally graded plates in thermal environments. *International Journal of Solids and Structures*, *41*(9–10), 2403–2427. https://doi.org/10.1016/j.ijsolstr.2003.11.012
8. Kalali, A.T., Hassani, B., & Hadidi-Moud, S. (2016). Elastic-plastic analysis of pressure vessels and rotating disks made of functionally graded materials using the isogeometric approach. *Journal of Theoretical and Applied Mechanics*, *54*(1), 113–125. https://doi.org/10.15632/jtam-pl.54.1.113
9. Kołakowski, Z., & Teter, A. (2016). Some aspects of dynamic coupled response of functionally graded thin-walled columns with square cross-sections under in-plane pulse compression. *Journal of Theoretical and Applied Mechanics*, *54*(2), 449–462. https://doi.org/10.15632/jtam-pl.54.2.449
10. Li, H.C., Pang, F.Z., Ren, Y., Miao, X.H., & Ye, K.F. (2019). Free vibration characteristics of functionally graded porous spherical shell with general boundary conditions by using first-order shear deformation theory. *Thin-Walled Structures*, *144*, Article 106331. https://doi.org/10.1016/j.tws.2019.106331
11. Liu, W.G., Shu, B., Guo, L.Q., & He, H.L. (2017). Impacts of thermal environment on modal frequency of FGM shells (in Chinese). *Journal of Vibration and Shock*, *36*(4), 127–131. https://doi.org/10.13465/j.cnki.jvs.2017.04.020
12. Loy, C.T., & Lam, K.Y. (1997). Vibration of cylindrical shells with ring support. *International Journal of Mechanical Sciences*, *39*(4), 455–471. https://doi.org/10.1016/S0020-7403(96)00035-5
13. Mallek, H., Mellouli, H., Ben Said, L., Wali, M., Dammak, F., & Alhadri, M. (2025). Porosity effects on nonlinear static performances of functionally graded shells considering thickness stretching. *Facta Universitatis, Series: Mechanical Engineering*, *23*(4), 827–860. https://doi.org/10.22190/FUME240920015M

14. Matsunaga, H. (2009). Free vibration and stability of functionally graded circular cylindrical shells according to a 2D higher-order deformation theory. *Composite Structures*, *88*(4), 519–531. https://doi.org/10.1016/j.compstruct.2008.05.019

15. Pillai, A.U., & Rahaman, M.M. (2026). A novel phase-field model for fatigue failure in functionally graded materials under thermo-mechanical loading. *Composite Structures*, *379*, Article 120003. https://doi.org/10.1016/j.compstruct.2025.120003

16. Reddy, J.N. (2000). Analysis of functionally graded plates. *International Journal for Numerical Methods in Engineering*, *47*(1–3), 663–684. https://doi.org/10.1002/(SICI)1097-0207(20000110/30)47:1/3<663::AID-NME787>3.0.CO;2-8

17. Shen, H.-S. (2012). Nonlinear vibration of shear deformable FGM cylindrical shells surrounded by an elastic medium. *Composite Structures*, *94*(3), 1144–1154. https://doi.org/10.1016/j.compstruct.2011.11.012

18. Wan, R.H., Liu, W.G., Chen, L., & Pang, L. (2025a). Analysis of traveling wave vibration of GNPs-reinforced bi-directional functionally graded rotating joined cylindrical-conical-cylindrical shells. *Acta Mechanica*, *236*(5), 3035–3053. https://doi.org/10.1007/s00707-025-04309-6

19. Wan, R.H., Liu, W.G., Cheng, L., & Pang, L. (2025b). Traveling wave vibration analysis of rotating reinforced functionally graded conical shells. *Journal of Mechanical Science and Technology*, *39*(5), 2417–2429. https://doi.org/10.1007/s12206-025-0402-3

20. Wang, Y.Q., Ye, C., & Zu, J.W. (2018). Identifying the temperature effect on the vibrations of functionally graded cylindrical shells with porosities. *Applied Mathematics and Mechanics*, *39*(11), 1587–1604. https://doi.org/10.1007/s10483-018-2388-6

21. Wang, Y.W., & Wu, D.F. (2017). Free vibration of functionally graded porous cylindrical shell using a sinusoidal shear deformation theory. *Aerospace Science and Technology*, *66*, 83–91. https://doi.org/10.1016/j.ast.2017.03.003

22. Wu, L. (2004). Thermal buckling of a simply supported moderately thick rectangular FGM plate. *Composite Structures*, *64*(2), 211–218. https://doi.org/10.1016/j.compstruct.2003.08.004

23. Xu, H.D., Wang, Y., Xu, Z.Q., & Yu, X.G. (2024). Gegenbauer-Ritz method for free vibration analysis of rotating functionally graded graphene reinforced porous composite stepped cylindrical shells with arbitrary boundary conditions. *Engineering Structures*, *303*, Article 117555. https://doi.org/10.1016/j.engstruct.2024.117555

24. Xue, Y.Q., Jin, G.Y., Zhang, C.Y., Han, X.H., & Chen, J. (2023). Free vibration analysis of functionally graded porous cylindrical panels and shells with porosity distributions along the thickness and length directions. *Thin-Walled Structures*, *184*, Article 110448. https://doi.org/10.1016/j.tws.2022.110448

Manuscript received December 29, 2025; accepted for publication July 16, 2026; published online August 17, 2026.